Precessional Motion in Crystalline Solid Solutions of Ionic Rotors

Precessional Motion in Crystalline Solid Solutions of Ionic Rotors.

Simone d'Agostino,[a] Luca Fornasari,[a] Fabrizia Grepioni,[a] Dario Braga,*[a] Federica Rossi,[b] Michele R. Chierotti[b] and Roberto Gobetto*[b]

Abstract: The order-disorder phase transition associated with the uprise of reorientational motion in $(DABCOH2)^{2+}$, in the supramolecular salts of general formula [**1**·$(DABCOH_2)$]X_2 (where **1** = 12-crown-4, DABCO = 1,4-diazabicyclo[2.2.2]octane, and X = Cl^- or Br^-), has been investigated by variable temperature X-ray diffraction on single crystals and powder samples, as well as by DSC and solid state NMR spectroscopy. The two compounds undergo a reversible phase change at 292 and 290 K, respectively. The two crystalline materials form solid solutions [**1**·$(DABCOH_2)$]$Cl_{2x}Br_{2(1-x)}$ in the whole composition range (0 < x <1), with a decrease in the temperature of transition to a minimum of ca 280 K corresponding to x = 0.5. Activation energies values for the dynamic processes evaluated by VT-^{13}CMAS-SSNMR and line-shape analysis are ca 50 kJmol^{-1} in all cases. Combined diffraction and spectroscopic evidence has allowed the detection of a novel dynamic process for the $(DABCOH_2)^{2+}$ dications, based on a room temperature precessional motion that is frozen out below the disorder-order transition; to the best of the authors' knowledge this phenomenon has never been observed before.

Introduction

Dynamic processes, such as rotation and vibration of molecules within crystals, have long attracted the attention of researchers. Partly because dynamical processes taking place in the crystalline state undermine the popular "static" perception of a crystal and partly, and more importantly, because the understanding, control, and exploitation of such movements can give access to new properties in functional materials. For example, rotation of molecules in crystals has been recently investigated for: thermal modulation of birefringence,[1] nonlinear optic properties,[2] switchable ferroelectrics,[3,4] gas and vapor sensors,[5,6] and dielectric constant modulation.[3]

Important factors responsible for dynamic processes of a given fragment (or molecule) within a crystalline material are molecular shape and nature of the functional groups on the surface. Molecules with protruding and/or "interacting" groups (e.g. hydrogen bonding) tend to be more easily "locked in place" by the surrounding molecules than molecules with approximate flat, spherical or cylindrical shape.[7] These factors also dictate the potential energy profile associated with the motion, which, in the case of flat and cylindrical molecules, will show minima every (2π/n)°, corresponding to the periodicity n of the idealized symmetry axis of the fragment.[8,9] Other factors will be the strength and type of bond used to anchor the rotating unit to the stator;[10] and the steric hindrance around the fragment involved, namely the constraints deriving from close packing, which can forbid, or limit significantly, the motional freedom. Temperature, however, can play a fundamental role, as constraints imposed by the packing can be loosened by an increase in temperature.[8] Therefore the ability to combine type and strength of the interactions around the chosen molecular fragment is crucial for a successful design of materials with "tunable" dynamic processes. To this scope several approaches have been proposed: covalent modification of the fragment with bulky substituents,[7,11–13] trapping within molecular macrocages[14–16] or porous frameworks,[5,17,18] and synthesis of co-crystals based on halogen bonding interactions.[19–21]

Recently, solid solutions of molecular materials have also become an attractive target in the design of functional materials. Crystalline solid solutions can be defined as non-stoichiometric multi-component crystals in which two, or even more, components combine homogeneously in a single crystalline phase. According to Kitaigorodsky,[22] formation of a solid solution, i.e. components miscibility in the solid state, depends on the similarity of the components in terms of size and shape. The pure components should, ideally, be isomorphous, or at least isostructural or *quasi*-isostructural.[22,23,§] The importance of solid solutions as a tool for modifying the physicochemical properties of materials has been recently emphasized in a series of studies on mixed crystals, where features such as melting point,[24,25] polymorphic phase transition,[26,27] enantioselectivity,[28,29] mechanical,[30] optical,[31] magnetic,[32] and thermosalient effects,[33] among others, can be studied and finely "tuned" by controlling the composition. This approach has also been successfully applied to control the rotational frequency of 4,4'-bpy rotators in porous coordination polymers.[34] Notwithstanding the extensive research in this field, two aspects have not yet been explored, namely (i) the possibility of obtaining dynamic crystalline materials *via* mechanochemistry,[35] and (ii) the effect of the solid solution composition on the transition temperature at which molecular motion stops.

In this work we have made use of crystal engineering[36,37] design principles for the preparation of supramolecular salts with general

[a] M.Sc. L. Fornasari, Dr. S. d'Agostino, Prof. F.Grepioni, Prof. D. Braga
Dipartimento di Chimica G. Ciamician, Università di Bologna
Via Selmi, 2, 40126 Bologna, Italy
dario.braga@unibo.it

[b] M. Sc. F. Rossi, Prof. M. R. Chierotti, Prof. R. Gobetto
Department of Chemistry and NIS Centre, University of Torino
Via Giuria 7, 10125 Torino, Italy
roberto.gobetto@unito.it

Supporting information for this article is given via a link at the end of the document.

formula [**1**·(DABCOH$_2$)]X$_2$, (where **1** = 12-crown-4, X = Cl$^-$ or Br$^-$), see scheme 1, in order to study the thermally activated dynamic processes occurring in their crystalline state. Moreover, by taking advantage of interchangeability between halides,[33,38] we have explored the preparation of binary solid solutions with general formula [**1**·(DABCOH$_2$)]Cl$_{2x}$Br$_{2(1-x)}$ (0 < x <1), to investigate the effect of composition on the disorder-order transition temperature and dynamic processes of the mixed systems with respect to the pure parent materials.

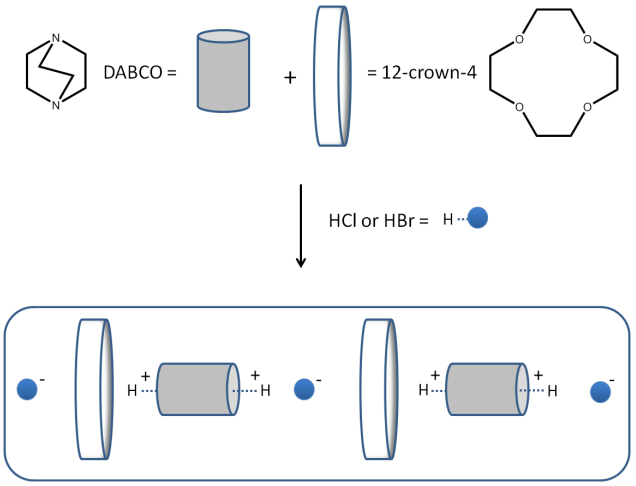

Scheme 1. Building blocks used in the present study and pathway to assemble the supramolecular salts.

The mixed crystals have been investigated by a combination of solid state techniques including variable temperature single crystal and powder X-ray diffraction (XRD), differential scanning calorimetry (DSC), hot stage microscopy (HSM) and solid-state NMR spectroscopy. The combined use of these methods has made possible not only to rationalize the correlation between the dynamic processes taking place within the crystalline materials and the solid solution composition, but also to describe an uncommon molecular motion based on a precession of the (DABCOH$_2$)$^{2+}$ unit within the cavity delimited in the crystal structure by the crown ether and the halide packing.

Results and Discussion

Crystal structures description

At room temperature crystalline [**1**·(DABCOH$_2$)]Cl$_2$ and [**1**·(DABCOH$_2$)]Br$_2$ are isomorphous; they crystallize in the tetragonal space group P4/n and form colourless square-like crystals (Figure SI-1). Both crystals feature infinite chains held by directional charge-assisted hydrogen bonds and running along the *c*-axis direction, in which each 12-crown-4 ether molecule is sandwiched between a (DABCOH$_2$)$^{2+}$ cationic unit and one halide anion, as shown in Figure 1. Each (DABCOH$_2$)$^{2+}$ cation, in turn, is surrounded by four *extra-chain* halide anions also interacting through weak C-H···X$^-$ hydrogen bonds (see Figure 1 and Table SI-1 for a list of distances).

Both crystals feature disorder of the (DABCOH$_2$)$^{2+}$ cation, likely due to the fast rotation about its *pseudo*-three-fold axis,[4,19] and of the 12-crown-4 molecule. According to the literature,[39–41] disorder in crown ethers is caused by the up-down flips of the -CH$_2$-CH$_2$- bridges (E$_a$ = 0.85 kJmol^{-1}) and by the *pseudo*-four-fold rotational jumps of the ring (E$_a$ = 40-50 kJmol^{-1}).

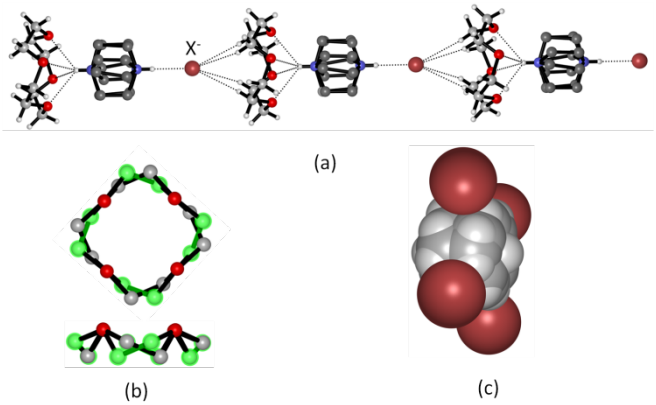

Figure 1. (a) The infinite hydrogen bonded chain in crystalline [**1**·(DABCOH$_2$)]Br$_2$, (b) top and side views of the disordered 12-crown-4 molecule (C atoms of the second image of disorder in green), and (c) the (DABCOH$_2$)$^{2+}$ dication surrounded by four bromide anions.

On decreasing the temperature both [**1**·(DABCOH$_2$)]Cl$_2$ and [**1**·(DABCOH$_2$)]Br$_2$ undergo a phase transition from tetragonal P4/n to monoclinic P2$_1$/n (see data at 200K in Table SI-2). Associated with this change in crystal symmetry it is possible to observe the ordering of the (DABCOH$_2$)$^{2+}$ cationic unit. This behavior indicates that one of the partially occupied sites at room temperature becomes more stable and fully occupied at low temperature, thus supporting a dynamic disorder model. The crown ether, on the contrary, is still disordered at low temperature. The disorder of (DABCOH$_2$)$^{2+}$ is perfectly restored when the crystalline samples are heated back to RT. DSC measurements (*vide infra*) also reveal that the two compounds undergo a reversible phase change at 292 and 290 K, respectively. A further evidence comes from the observation of birefringence variation at the Cross-Polarized Hot Stage Microscope (see Figure 2 and the Video in SI).

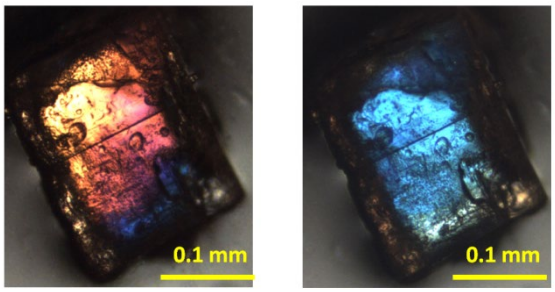

Figure 2. Cross-polarized HSM pictures showing the change in birefringence in a crystal of [**1**·(DABCOH$_2$)]Br$_2$ before (left) and after (right) the disorder-to-order/tetragonal-to-monoclinic phase transition.

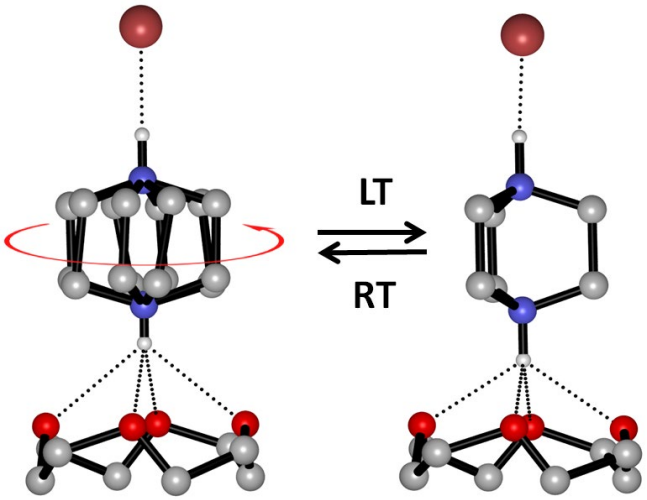

Figure 3. Representation of the fully reversible interconversion between the RT and LT phases for [**1**·(DABCOH$_2$)]Br$_2$. H_{CH} and disorder over the 12-crown-4 omitted for clarity.

Single crystals of the two salts were also subjected to an additional cooling cycle down to 100K on the diffractometer. Only slight shrinking in the values of the unit cell parameters was observed for both solids, but no further phase transition was detected.

Solid solutions

The observed dynamic behavior as a response to temperature variation, and the isomorphism of [**1**·(DABCOH$_2$)]Cl$_2$ and [**1**·(DABCOH$_2$)]Br$_2$ in both their room temperature and low temperature phases, prompted us to investigate the possibility of obtaining mixed-crystal phases. More specifically, we set to address the following questions:

i) would the two salts form a solid solution or separate out in crystals of the two salts?
ii) If a solid solution is formed from solution crystallization would it be possible to obtain the same result via mechanochemistry?
iii) how could alloy formation affect the phase transition behavior depending on the Cl^- / Br^- molar ratio? i.e. Would the phase transition temperature vary linearly as a function of the molar ratio, between the two extremes defined by the homo-anionic crystals, or not?

Mixed crystalline phases were successfully obtained from slow evaporation of water solutions containing [**1**·(DABCOH$_2$)]Cl$_2$ and [**1**·(DABCOH$_2$)]Br$_2$ in the molar ratios: 90:10, 75:25, 50:50, 25:75, 10:90. Alternatively they can be obtained via kneading (few drops of water) of the reactants in the same molar ratio. While dry grinding afforded a simple mixture of the two starting phases.

Powder diffraction patterns, recorded on materials obtained via kneading, showed a clear-cut proof of solid phases formation isomorphous with those of pure [**1**·(DABCOH$_2$)]Cl$_2$ and [**1**·(DABCOH$_2$)]Br$_2$ in all cases. Figure 4 shows a detail of the comparison between experimental PXRD patterns of the parent materials and that of the kneaded phase with a 50: 50 ratio, e.g. [**1**·(DABCOH$_2$)].

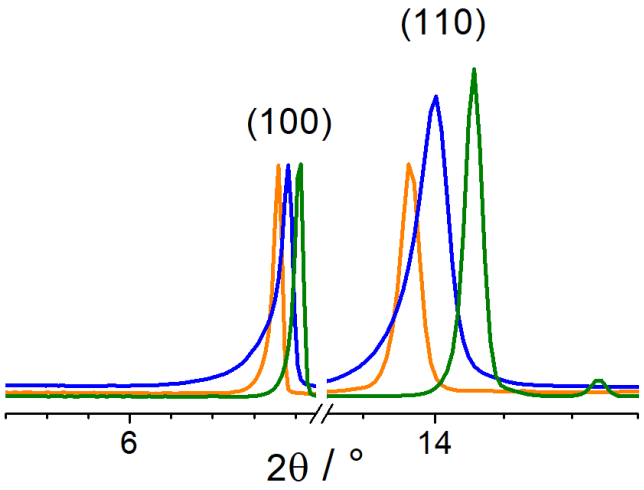

Figure 4. Details of the PXRD patterns showing the shifts of the (100) and (110) peaks towards higher angles upon increasing the molar fraction of Cl^-. [**1**·(DABCOH$_2$)]Br$_2$ orange line, [**1**·(DABCOH$_2$)]ClBr blue line, and [**1**·(DABCOH$_2$)]Cl$_2$ green line.

Based on a comparison of the unit cell volumes extracted from Pawley refinements, the two supramolecular salts are indeed miscible, affording crystalline phases that follow Vegard's rule[42] in the whole composition range (see Figure 5) and can be indeed formulated as [**1**·(DABCOH$_2$)]Cl$_{2x}$Br$_{2(1-x)}$ (with 0 < x <1).

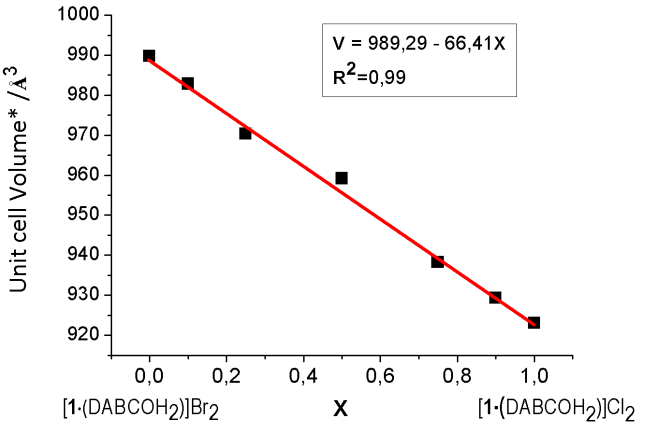

Figure 5. Linear dependence of unit cell volume (data from Pawley refinements) on the molar fraction of Cl^- in [**1**·(DABCOH$_2$)]Cl$_{2x}$Br$_{2(1-x)}$.

To determine the temperatures associated with the disorder-order phase transitions, each [**1**·(DABCOH$_2$)]Cl$_{2x}$Br$_{2(1-x)}$ crystalline powder was subjected to a full cycle (cooling-heating-cooling) of differential scanning calorimetry (DSC) measurements. The measurements were carried out below the thermal decomposition corresponding to the crown ether loss (see Figure SI-3). Figure 6 shows the plot of transition temperatures vs. composition.

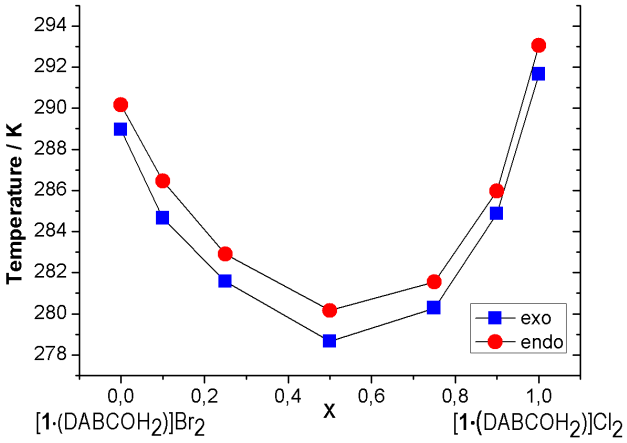

Figure 6. Temperature variations (from DSC, peak temperatures) of the disorder-order transition for [**1**·(DABCOH$_2$)]Cl$_{2x}$Br$_{2(1-x)}$ with x = 0, 0.1, 0.25, 0.5, 0.75, 0.90, and 1.

As in the cases of the pure materials, the transitions are fully reversible and with some hysteresis. Moreover, the DSC traces showed how the phase transition behavior does not vary linearly with the composition and how the peak corresponding to the disorder-order transition "drops" as the molar fraction of Cl^- is changed, reaching a minimum for x = 0.5.

To dispel any doubt concerning the disorder-order transition we carried out also single crystal analyses in the before and after the DSC peak for [**1**·(DABCOH$_2$)]Cl$_{2x}$Br$_{2(1-x)}$ with x = 0, 1, and 0.5 (see Figure 7). This experiment confirms what formerly observed at RT and LT for each phase. Transition enthalpies (ΔH) for the disorder-order transition were estimated to be of *ca* -1.0 kJ·mol^{-1} for all crystalline phases. This might imply that reorientation of the (DABCOH$_2$)$^{2+}$ cationic unit is substantially unaffected by the type of the surrounding halide anion.

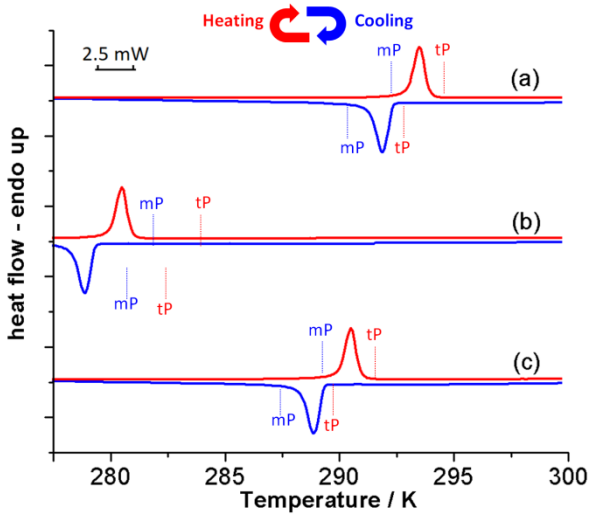

Figure 7. DSC traces measured on [**1**·(DABCOH$_2$)]Cl$_{2x}$Br$_{2(1-x)}$: (a) x = 1, (b) x = 0.5, and (c) x = 0. tP and mP stand for the disordered (tetragonal P) and ordered (monoclinic P) crystal phases, respectively.

Further evidence of the reversible phase transition comes from variable temperature X-ray powder diffraction. Figure 8 shows the changes in the XRD pattern for [**1**·(DABCOH$_2$)]Br$_2$] observed upon cooling a polycrystalline sample below the transition temperature. [**1**·(DABCOH$_2$)]Cl$_2$] and [**1**·(DABCOH$_2$)]ClBr] behave similarly, see Figure SI-5.

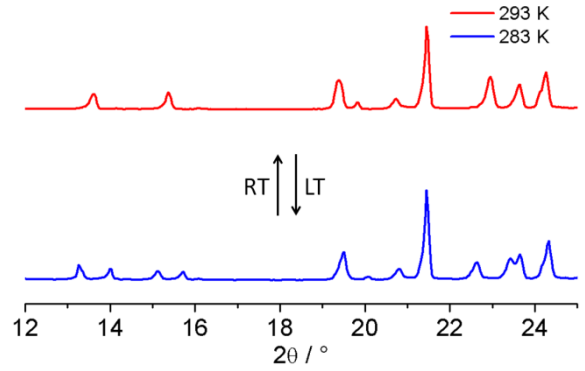

Figure 8. Details of the variable temperature PXRD patterns of [**1**·(DABCOH$_2$)]Br$_2$]; the phase transition occurring upon lowering the temperature is visible from the marked change of the peaks at ca. 13, 15 and 24 °.

Solid State NMR - Dynamics

The SSNMR measurements were instrumental to the elucidation of the dynamic processes. Interestingly, ^{13}C CPMAS spectra of [**1**·(DABCOH$_2$)]Cl$_2$, [**1**·(DABCOH$_2$)]Br$_2$ and [**1**·(DABCOH$_2$)]ClBr at room temperature afforded only the DABCO-CH$_2$ peak (around 45 ppm), thus ^{13}C MAS spectra were acquired. Figure 9 shows ^{13}C MAS SSNMR spectra of [**1**·(DABCOH$_2$)]Cl$_2$, [**1**·(DABCOH$_2$)]Br$_2$ and [**1**·(DABCOH$_2$)]ClBr at room temperature.

For the three samples, two different signals were observed at 45.2 and 66.4 ppm assigned to the $–CH_2$ groups of $(DABCOH_2)^{2+}$ and 12-crown-4, respectively. The lack of the crown ether CH_2 signals in the ^{13}C CPMAS spectra together with short ^{13}C relaxation delays, the large line width of the 12-crown-4 signal (FWHM = 200-340 Hz) as well as the need of acquiring MAS experiments on solid samples, confirm the presence of dynamic processes. This prompted us to perform variable temperature (VT) NMR measurements.

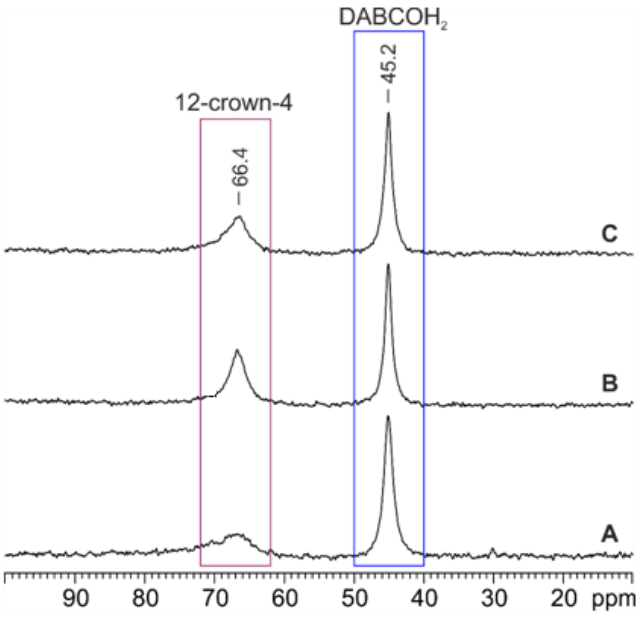

Figure 9. Room temperature ^{13}C (150.9 MHz) MAS SSNMR spectra of A) [**1**·$(DABCOH_2)$]Cl_2, B) [(**1**·$(DABCOH_2)$]Br_2 and C) [**1**·$(DABCOH_2)$]ClBr acquired at a spinning speed of 20 kHz.

The ^{13}C MAS spectra of [**1**·$(DABCOH_2)$]Cl_2 recorded at different temperature values, from 253 to 323 K, are reported in Figure 10.

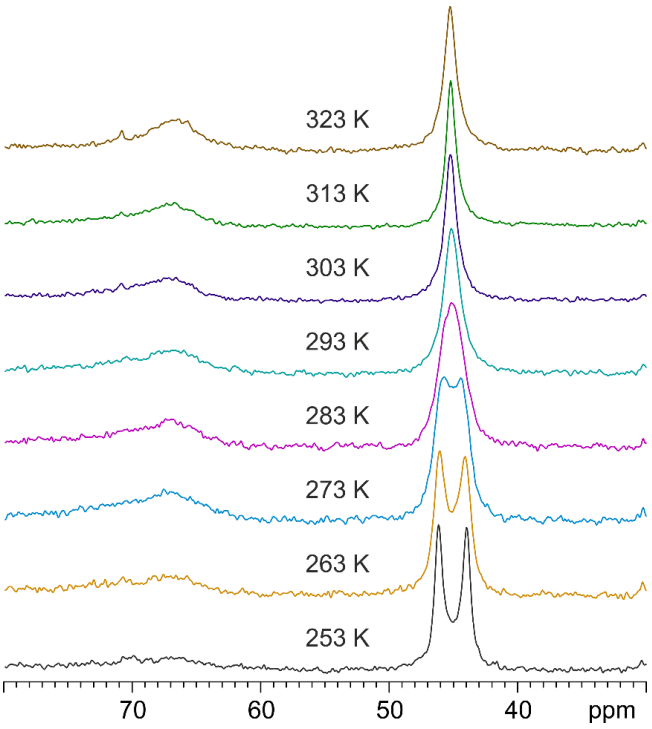

Figure 10. VT ^{13}C (150.9 MHz) MAS SSNMR spectra of [(**1**·$(DABCOH_2)$]Cl_2, acquired at a spinning speed of 20 kHz.

By changing the temperature, the crown ether signal does not change significantly as it is disordered at all temperatures in agreement with the X-ray data (see above). On the other hand, the resonance at lower ppm undergoes a significant change: two distinct resonances are observed at low temperatures (44.0 and 46.2 ppm); as the temperature is increased, the two signals coalesce and merge as a single signal centred at 45.3 ppm, whereas no significant change is observed for the high-frequency CH_2 resonance. The coalescence temperature is around 278 K. From the VT spectra it is clear that RT and LT structures are very similar from the NMR point of view. The differences stem on the features related to the dynamic process, rather than the phase transition.

Similar response is observed for both [**1**·$(DABCOH_2)$]Br_2 and [**1**·$(DABCOH_2)$]ClBr, (see Figures SI-6 and SI-7 in Supporting Information). In these cases, however, the coalescent temperature is around 268 K suggesting a lower activation energy.

The activation energies for the dynamic processes can be evaluated by lineshape analysis and values of 52.7, 50.6 and 50.6 $kJmol^{-1}$ are obtained for [**1**·$(DABCOH_2)$]Cl_2, [**1** ·$(DABCOH_2)$]Br_2 and [**1**·$(DABCOH_2)$]ClBr, respectively.

In order to evaluate if the hydrogen atom is involved in the dynamic, the deuterium analogous of [**1**·$(DABCOH_2)$]Cl_2 was synthesized (see Experimental Section). Figure SI-8 shows the comparison between the VT ^{13}C MAS spectra of [**1**·$(DABCOH_2)$]Cl_2 and [**1**·$(DABCOD_2)$]Cl_2 in the 193-313K range. We found a different coalescence temperature: 278 K for the hydrogen derivative and 293 K for the deuterium analogue,

suggesting the presence of a kinetic isotopic effect. The corresponding calculated activation energy for [**1**·(DABCOH$_2$)]Cl$_2$ is 58.5 kJmol^{-1}. The kinetic isotope effect, K_H/K_D, measured at 293 K is 5.3. It is well known that deuterium substitution will lead to lower vibration frequencies or, viewed quantum-mechanically, will have lower zero-point energy. With a lower zero-point energy, more energy must be supplied to break the bond, resulting in a higher activation energy for bond cleavage, which in turn lowers the measured exchange rate.[43] This relevant kinetic isotope effect confirms that the hydrogen atom bound to the nitrogen plays a role on the dynamic under investigation.

The rotation of DABCO unit along its pseudo-three-fold axis has been already reported in several cases in the literature[4,19] and accounts for the short ^{13}C relaxation delays (< 5s). Such motion is expected to have a very low activation energy and cannot be frozen at the lowest achievable NMR temperature. Thus, the reported behavior upon varying the temperature suggests the presence of a second dynamic process which accounts for the loss of symmetry of the DABCO-CH$_2$ which, at low temperature, gives rise to two distinct peaks. Such large chemical shift difference of the CH$_2$ resonances cannot be related to the presence of the halide and the crown ether along the (DABCOH$_2$)$^{2+}$ axis. For example, no chemical shift difference has been found in the case of the ^{13}C CPMAS spectrum of the adduct between DABCO and malonic acid where one of the nitrogen forms a strong hydrogen bond with the carboxylic acid, whereas the other is a free nitrogen.[44] Thus, the difference in the CH$_2$ resonances at low temperature is probably due to the presence of the surrounding four halides. Beside the rotation of the (DABCOH$_2$)$^{2+}$, we surmise an additional precession motion of the cationic unit around its principal axis at room temperature (see Scheme 2), during which the N$^+$-H moiety interacts in turn with each oxygen atom of the crown ether. This would explain also the presence of the kinetic isotope effect that is related to the breaking and forming of the N$^+$-H···O$_{crown}$ or N$^+$-D···O$_{crown}$ interactions in [**1**·(DABCOH$_2$)]Cl$_2$ and [**1**·(DABCOD$_2$)]Cl$_2$. This agrees with the slight (DABCOH$_2$)$^{2+}$ misalignment (ca 1-2°) between the (DABCOH$_2$)$^{2+}$ *pseudo*-threefold axis and the crown ether pseudo-fourfold axis, which leads to slightly shorter N$^+$-H···O$_{crown}$ distances as observed in the low temperature X-ray structure (see Table SI-1).

By performing such motion, the two different -CH$_2$- groups of the rotating (DABCOH$_2$)$^{2+}$ change their position with respect to the surrounding four halides, averaging their relative environment in the RT range and leading to the single peak observed on the VT ^{13}C MAS spectra.

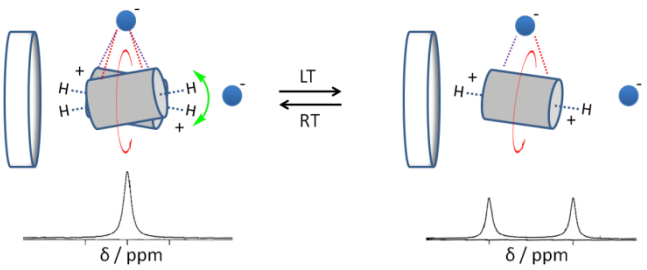

Scheme 2. Representation of the dynamic model inferred from VT ^{13}C MAS SSNMR experiments showing the precession motion that accompanies the rotation of the (DABCOH$_2$)$^{2+}$ around its pseudo-three-fold axis, and the slight misalignment which causes signal coalescence loss following the phase transition.

Conclusions

In this paper we have reported our findings on the solid state dynamic behavior and phase transition of the supramolecular salts of general formula [**1**·(DABCOH$_2$)]X$_2$ (where **1** = 12-crown-4; X = Cl$^-$ or Br$^-$) and of their solid solutions, namely [**1**·(DABCOH$_2$)]Cl$_{2x}$Br$_{2(1-x)}$. These latter compounds were prepared mechanochemically by mixing the parent compounds in different stoichiometric rations.

Our findings can be summarized as follows: i) the salts [**1**·(DABCOH$_2$)]X$_2$ are isostructural and their crystals are isomorphous; ii) both compounds undergo a reversible order-disorder enantiotropic transition from a higher to a lower symmetry phase at temperatures close to RT (292 and 290 K, for x = 1and 0, respectively); iii) their solid solutions also undergo the same kind of phase transition and show a coherent decrease of the transition temperatures with a minimum at 278K corresponding to the composition Cl:Br 1:1; iv) the order-disorder phase transitions, investigated by a combination of X-ray diffraction and solid state NMR spectroscopy, are associated with the uprise of reorientational motion of the (DABCOH2)$^{2+}$ dications within a "cage", formed by one (12-crown-4) molecule on one side and a halide ion on the other side and by four surrounding halide ions; v) the solid solutions behave exactly in the same way, confirming that the dynamic process involves the mobile (DABCOH2)$^{2+}$dication; vi) activation energies of ca 50 kJmol^{-1}, associated in all cases to the dynamic processes, have been evaluated by VT ^{13}C MAS SSNMR and line-shape analysis.

We have argued that a simple rotation of the DABCO core around the molecular threefold axis, as observed in many other DABCO containing crystals, cannot account for the spectroscopic evidence, whereas a more complex precessional motion could explain the differences between high and low temperature solid state structures, the small enthalpy involved in the fully reversible processes, and the intriguing spectroscopic features discussed above.

The compound 1,4-diazabicyclo[2.2.2]octane, DABCO, is most certainly a very popular, and extensively investigated mobile molecular fragment. However, to the best of the authors' knowledge, this is the first observation of a room temperature precessional motion that is frozen as the hosting cage is made tighter by decreasing the temperature.

Experimental Section

All reactants and reagents were purchased from Sigma-Aldrich and used without further purification, bidistilled water was used.

Synthesis

1,4-diazabicyclo[2.2.2]octane (DABCO) and 12-crown-4 were mixed together in stoichiometric ratio 1: 1. Hydrochloric or hydrobromic acid were added dropwise up to reach pH = 5. The resulting solution was boiled for a few minutes and left to stand in the air at room temperature. After a few days single crystals of [**1**·(DABCOH$_2$)]X$_2$ (X = Cl$^-$ or Br$^-$) grew from solution; they were collected by filtration and washed with cold ethanol. [**1**·(DABCOD$_2$)]Cl$_2$ was obtained by using deuterium chloride (DCl) instead of HCl; the obtained crystals were washed with EtOH-d6.

Solid solutions were prepared by kneading quantities of pure [**1**·(DABCOH$_2$)]Cl$_2$ and [**1**·(DABCOH$_2$)]Br$_2$ weighed in the proper molar ratio (10:90, 25:75, 50:50, 75:25, 91:10) and in the presence of few drops of water; alternatively they could be obtained by slow evaporation of an aqueous solution. The amount of reagents for each synthesis was chosen so that ca. 100-200 mg of solid product could be obtained.

Single Crystal X-ray Diffraction

Single-crystal data for all supramolecular salts were collected either at RT (300K) and LT (200 K) on an Oxford X'Calibur S CCD diffractometer equipped with a graphite monochromator (Mo-Kα radiation, λ = 0.71073 Å) and with a cryostat Oxford CryoStream800. Data collection and refinement details are listed in *SI-Table 1*. All non-hydrogen atoms were refined anisotropically. H_{CH} atoms were added in calculated positions and refined riding on their respective carbon atoms; H_{NH} atoms were either directly located or, when not possible, added in calculated positions. The structures were solved with SHELXT[45] and refined on full-matrix F^2 by means of SHELXL package[46], implemented in Olex2 software[47].

The data collected at RT showed disordered positions for the CH_2 atoms belonging to both DABCO and crown ether. Methylene atoms of the crown ether were split over two conformations with occupancies fixed at 0.5; where necessary, their thermal parameters were restrained using ISOR and/or SIMU and DELU instructions. Since the disorder involving DABCO is roughly continuous, a fictitious molecule comprising four methylene bridges is generated by the fourfold symmetry imparted by the crown ether. The CH_2 atoms in the model were then further split over two different conformations fixing their occupancies at (3/4)/2 = 0.375; because of the strong elongation, their thermal parameters were restrained using ISOR and SIMU instructions, while the corresponding hydrogen atoms were omitted.

All the LT data displayed crystal twinning. [(**1**·(DABCOH$_2$)]Br$_2$ and [(**1**·(DABCOH$_2$)]BrCl were treated with the default configuration for twinned crystals of CrysAlisPro, and structure solution and refinement were performed on the HKLF4 file containing the non-overlapped reflections; due to the strong overlapping, [(**1**·(DABCOH$_2$)]Cl$_2$ was instead treated as a single crystal and the size of the integration mask was increased by 25%. In all cases the crown ethers were disordered and they were treated as detailed above for RT data.

In the structures of [(**1**·(DABCOH$_2$)]BrCl it was not always possible to unequivocally locate from the Fourier maps the independent positions of the two anions. In this case, the model was approximated forcing a fictious atom possessing the scattering factor of Co, which corresponds to the number of electrons of an ideal atom with composition Cl0.5Br0.5. Where two independent positions were visible Cl and Br atoms were refined with 0.5 occupancy.

The program Mercury 3.1 was used to calculate intermolecular interactions and for molecular graphics. Crystal data can be obtained free of charge via www.ccdc.cam.ac.uk/conts/retrieving.htmL (or from the Cambridge Crystallographic Data Centre, 12 Union Road, Cambridge CB21EZ, UK; fax: (+44)1223-336-033; or e-mail: deposit@ccdc.cam.ac.uk). CCDC numbers 1849206-1849211.

Powder X-ray Diffraction

For phase identification and Pawley refinement purposes X-ray powder diffraction patterns (XRPD) were collected on a PANalytical X'Pert PRO automated diffractometer with transmission geometry equipped with Focusing Mirror and Pixcel detector in the 2θ range 3–70° (step size 0.0260°, time/step 200 s, 0.04 rad soller; VxA 40kV x 40mA). Powder diffraction data were analyzed with the software TOPAS4.1.[48] A shifted Chebyshev function with 7 parameters was used to fit the background.

Thermogravimetric analysis (TGA)

TGA analyses were performed with a Perkin-Elmer TGA-7. Each sample, contained in a platinum crucible, was heated in a nitrogen flow (20 cm3 min$_{-1}$) at a rate of 5°C min$_{-1}$, up to decomposition. Samples weights were in the range 5–10 mg.

Differential scanning calorimetry (DSC)

Calorimetric measurements were performed with a Perkin-Elmer DSC-7 equipped with a PII intracooler. Temperature and enthalpy calibrations were performed using high-purity standards (n-decane, benzene and indium). Heating of the aluminium open pans containing the samples (3–5 mg) was carried out at 5 °C min^{-1} in the temperature range 40–300°C.

Hot Stage and Cross-polarized Optical Microscopy (HSM-CP)

Hot Stage experiments were carried out using a Linkam TMS94 device connected to a Linkam LTS350 platinum plate and equipped with polarizing filters. Images and movies were collected with the imaging software VisiCam Analyzer, from an Olympus BX41 stereomicroscope.

Solid-State NMR

1D ^{13}C MAS spectra were acquired on a Jeol ECZR 600 instrument, operating at 600.17 and 150.91 MHz for the ^{1}H and ^{13}C nuclei, respectively. Powder samples were packed in 3.2 mm diameter cylindric zirconia rotors with a volume of 60 μL. A certain amount of sample was taken and used without further preparation from each batch to fill the rotor. ^{13}C MAS spectra were acquired at a spinning speed of 20 kHz with a 90° ^{13}C pulse of 2.0 μs, a recycle time of 10 s and 64 scans. The two-pulse phase modulation (TPPM) decoupling scheme with a 119.0 kHz radiofrequency field was used. ^{13}C chemical shifts were referenced to glycine (^{13}C methylene signal at respectively).

Variable-temperature operation was achieved by a triple gas channel MAS probe, in which the stream of VT gas is separated from the MAS bearing and driving gases. The driving gas is used to propel the rotor at high speeds, while the bearing gas provides an air cushion for stability. The low temperatures were achieved by cooling the VT line through a flow of boil-off N_2 gas from an exchange dewar filled with liquid nitrogen. The VT gas was then directed at the mid-point of the sample rotor. For the high temperature operations, VT and MAS gases were air heated by means of a resistance put inside the probe.
A thermocouple was used for temperature measurement and regulation. The temperature was calibrated using the well-established method based on the ^{207}Pb NMR resonance of solid Pb(NO$_3$)$_2$.[49–52]

Acknowledgements

Financial support by the Universities of Bologna and Torino is gratefully ackowledged. F.R. thanks Jeol (Italia) S.p.A. for a Ph.D. scholarship.

Keywords: molecular motion in crystals • crystalline solid solutions • crystal engineering • mechanochemistry

§ = Two crystals are said to be isomorphous if (*a*) both have the same space group and unit-cell dimensions and (b) the types and the positions of atoms in both are the same except for a replacement of one or more atoms in one structure with different types of atoms in the other (diadochy), such as heavy atoms, or the presence of one or more additional atoms in one of them (*isomorphous addition*). Isomorphous crystals can form *solid solutions*. Two crystals are said to be isostructural if they have the same structure, but not necessarily the same cell dimensions nor the same chemical composition, and with a 'comparable' variability in the atomic coordinates to that of the cell dimensions and chemical composition. The term isotypic is synonymous with isostructural.

[1] W. Setaka, K. Yamaguchi, *Proc. Natl. Acad. Sci.* **2012**, *109*, 9271–9275.

[2] Z. Sun, J. Luo, S. Zhang, C. Ji, L. Zhou, S. Li, F. Deng, M. Hong, *Adv. Mater.* **2013**, *25*, 4159–4163.

[3] T. Akutagawa, H. Koshinaka, D. Sato, S. Takeda, S. Noro, H. Takahashi, R. Kumai, Y. Tokura, T. Nakamura, *Nat. Mater.* **2009**, *8*, 342–347.

[4] A. Katrusiak, M. Szafrański, *Phys. Rev. Lett.* **1999**, *82*, 576–579.

[5] S. Bracco, M. Beretta, A. Cattaneo, A. Comotti, A. Falqui, K. Zhao, C. Rogers, P. Sozzani, *Angew. Chemie - Int. Ed.* **2015**, *54*, 4773–4777.

[6] S. Bracco, F. Castiglioni, A. Comotti, S. Galli, M. Negroni, A. Maspero, P. Sozzani, *Chem. - A Eur. J.* **2017**, *23*, 11210–11215.

[7] S. D. Karlen, R. Ortiz, O. L. Chapman, M. A. Garcia-Garibay, *J. Am. Chem. Soc.* **2005**, *127*, 6554–6555.

[8] D. Braga, *Chem. Rev.* **1992**, *92*, 633–665.

[9] C. S. Vogelsberg, M. A. Garcia-Garibay, *Chem. Soc. Rev.* **2012**, *41*, 1892–1910.

[10] C. S. Vogelsberg, F. J. Uribe-romo, A. S. Lipton, S. Yang, K. N. Houk, S. Brown, **2017**, 2–7.

[11] Z. J. Obrien, S. D. Karlen, S. Khan, M. A. Garcia-Garibay, *J. Org. Chem.* **2010**, *75*, 2482–2491.

[12] Z. J. O'Brien, A. Natarajan, S. Khan, M. A. Garcia-Garibay, *Cryst. Growth Des.* **2011**, *11*, 2654–2659.

[13] P. Commins, M. A. Garcia-Garibay, *J. Org. Chem.* **2014**, *79*, 1611–1619.

[14] A. Fujiwara, Y. Inagaki, H. Momma, E. Kwon, K. Yamaguchi, M. Kanno, H. Kono, W. Setaka, *CrystEngComm* **2017**, *19*, 6049–6056.

[15] W. Setaka, S. Higa, K. Yamaguchi, *Org. Biomol. Chem.* **2014**, *12*, 3354–3357.

[16] Y. Nishiyama, Y. Inagaki, K. Yamaguchi, W. Setaka, *J. Org. Chem.* **2015**, *80*, 9959–9966.

[17] A. Comotti, S. Bracco, P. Sozzani, *Acc. Chem. Res.* **2016**, *49*, 1701–1710.

[18] S. Devautour-Vinot, G. Maurin, C. Serre, P. Horcajada, D. Paula Da Cunha, V. Guillerm, E. De Souza Costa, F. Taulelle, C. Martineau, *Chem. Mater.* **2012**, *24*, 2168–2177.

[19] (a) L. Catalano, S. Pérez-Estrada, G. Terraneo, T. Pilati, G. Resnati, P. Metrangolo, M. A. Garcia-Garibay, *J. Am. Chem. Soc.* **2015**, *137*, 15386–15389. (b) L. Catalano, P. Naumov, *CrystEngComm*, **2018**, 10.1039/C8CE00420J

[20] L. Catalano, S. Perez-Estrada, H. Wang, A. J.-L. Ayitou, S. I. Khan, G. Terraneo, P. Metrangolo, S. Brown, M. A. Garcia-Garibay, *J. Am. Chem. Soc.* **2017**, *139*, 843–848.

[21] C. Lemouchi, C. S. Vogelsberg, L. Zorina, S. Simonov, P. Batail, S. Brown, M. A. Garcia-Garibay, *J. Am. Chem. Soc.* **2011**, *133*, 6371–6379.

[22] A. I. Kitaigorodsky, *Mixed Crystals*, Springer Berlin Heidelberg, Berlin, Heidelberg, **1984**.

[23] M. Lusi, *Cryst. Growth Des.* **2018**, acs.cgd.7b01643.

[24] A. K. S. Romasanta, D. Braga, M. T. Duarte, F. Grepioni, *CrystEngComm* **2017**, *19*, 653–660.

[25] E. Schur, E. Nauha, M. Lusi, J. Bernstein, *Chem. - A Eur. J.* **2015**, *21*, 1735–1742.

[26] D. Braga, D. Paolucci, G. Cojazzi, F. Grepioni, *Chem. Commun.* **2001**, 803–804.

[27] A. Delori, P. Maclure, R. M. Bhardwaj, A. Johnston, A. J. Florence, O. B. Sutcliffe, I. D. H. Oswald, *CrystEngComm* **2014**, *16*, 5827.

[28] T. Rekis, S. d'Agostino, D. Braga, F. Grepioni, *Cryst. Growth Des.* **2017**, acs.cgd.7b01146.

[29] T. Rekis, A. Berziņš, I. Sarceviča, A. Kons, M. Balodis, L. Orola, H. Lorenz, A. Actiņš, *Cryst. Growth Des.* **2018**, *18*, 264–273.

[30] M. K. Mishra, U. Ramamurty, G. R. Desiraju, *J. Am. Chem. Soc.* **2015**, *137*, 1794–1797.

[31] L. Kuroki, S. Takami, K. Shibata, M. Irie, *Chem. Commun.* **2005**, 6005.

[32] R. D. Willett, R. E. Butcher, C. P. Landee, B. Twamley, *Polyhedron* **2006**, *25*, 2093–2100.

[33] E. Nauha, P. Naumov, M. Lusi, *CrystEngComm* **2016**, *18*, 4699–4703.

[34] M. Inukai, T. Fukushima, Y. Hijikata, N. Ogiwara, S. Horike, S. Kitagawa, *J. Am. Chem. Soc.* **2015**, *137*, 12183–12186.

[35] D. Braga, L. Maini, F. Grepioni, *Chem. Soc. Rev.* **2013**, *42*, 7638.

[36] D. Braga, F. Grepioni, A. G. Orpen, *Crystal Engineering: From Molecules and Crystals to Materials*, Springer Netherlands, Dordrecht, **1999**.

[37] D. Braga, F. Grepioni, L. Maini, S. D'Agostino, *IUCrJ* **2017**, *4*, 369–379.

[38] C. J. Adams, M. F. Haddow, M. Lusi, A. G. Orpen, *Proc. Natl. Acad. Sci.* **2010**, *107*, 16033–16038.

[39] C. I. Ratcliffe, J. A. Ripmeester, G. W. Buchanan, J. K. Denike, *J. Am. Chem. Soc.* **1992**, *114*, 3294–3299.

[40] C. I. Ratcliffe, G. W. Buchanan, J. K. Denike, *J. Am. Chem. Soc.* **1995**, *117*, 2900–2906.

[41] G. W. Buchanan, A. Moghimi, C. I. Ratcliffe, *Can. J. Chem.* **1996**, *74*, 1437–1446.

[42] A. R. Denton, N. W. Ashcroft, *Phys. Rev. A* **1991**, *43*, 3161–3164.

[43] A. Kohen, *Prog. React. Kinet. Mech.* **2003**, *28*, 119–156.

[44] D. Braga, L. Maini, G. De Sanctis, K. Rubini, F. Grepioni, M. R.

Chierotti, R. Gobetto, *Chem. - A Eur. J.* **2003**, *9*, 5538–5548.

[45] G. M. Sheldrick, *Acta Crystallogr. Sect. A Found. Crystallogr.* **2015**, *71*, 3–8.

[46] G. M. Sheldrick, *Acta Crystallogr. Sect. C Struct. Chem.* **2015**, *71*, 3–8.

[47] O. V Dolomanov, L. J. Bourhis, R. J. Gildea, J. A. K. Howard, H. Puschmann, *J. Appl. Crystallogr.* **2009**, *42*, 339–341.

[48] A. Cohelo, **2007**.

[49] A. Bielecki, D. P. Burum, *J. Magn. Reson. Ser. A* **1995**, *116*, 215–220.

[50] L. C. M. van Gorkom, J. M. Hook, M. B. Logan, J. V. Hanna, R. E. Wasylishen, *Magn. Reson. Chem.* **1995**, *33*, 791–795.

[51] T. Takahashi, H. Kawashima, H. Sugisawa, Toshihide Baba, *Solid State Nucl. Magn. Reson.* **1999**, *15*, 119–123.

[52] X. Guan, R. E. Stark, *Solid State Nucl. Magn. Reson.* **2010**, *38*, 74–76.

Entry for the Table of Contents

FULL PAPER

The solid state dynamic behavior and phase transition of the supramolecular salts of general formula [**1**·(DABCOH$_2$)]X$_2$ (where **1** = 12-crown-4; X = Cl$^-$ or Br$^-$) and of their solid solutions [**1**·(DABCOH$_2$)]Cl$_2$xBr$_{2(1-x)}$ is investigated by a combination of solid state techniques.

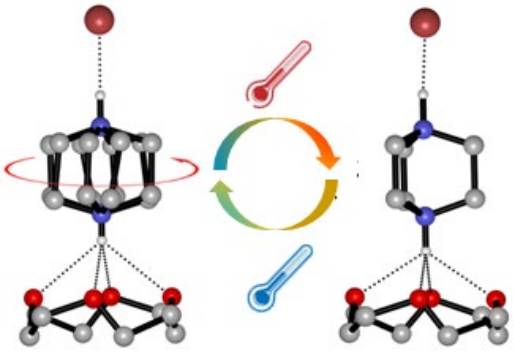

Simone d'Agostino, Luca Fornasari, Fabrizia Grepioni, Dario Braga, Federica Rossi, Michele R. Chierotti and Roberto Gobetto **

Page No. – Page No.

Precessional Motion in Crystalline Solid Solutions of Ionic Rotors